will widely cover the surface of the catalyst under methanol synthesis conditions. If more Zn atoms are considered in the CuZn(211) surface, the binding to these species is further strengthened (Fig. 2). According to this trend and in agreement with the higher oxophilicity of Zn compared with Cu, these species will bind to the surface via Zn atoms, leading to a formal oxidation of the Zn component. Thus, under steady-state conditions, the oxidation state of Zn is adjusted to a partially oxidized $Zn^{\delta+}$ state, which can be formed by reduction from the ZnO particles through SMSI as well as from a CuZn surface alloy by adsorbate-induced oxidation. The unique role of ZnO in the industrial catalyst is probably related to the stability of this intermediate oxidation state under the reducing potential of methanol synthesis conditions. Its reducibility is high enough to allow for partial reduction but sufficiently low not to favor bulk alloying. Other promoters that bind oxygen in the same range as Zn may have a similar effect. The Cu/ZrO_2 system, for example, is also an active methanol synthesis catalyst (*34*).

Combining the experimental and theoretical results, a model for the active site of methanol synthesis over industrial catalysts emerges. Undistorted pure Cu was quite inactive in the methanol synthesis experiment. The same result was obtained for the flat Cu(111) surface in the DFT calculations. High activity was generated by two factors. First, the presence of steps at the Cu surface is required, which can be stabilized by bulk defects like stacking faults or twin boundaries terminating at the surface. The increase in activity is explained by a stronger binding of the intermediates on stepped sites and lower energy barriers between them. The bulk defect structure in the real catalyst is a result of a well-optimized low-temperature preparation method.

The second requirement is the presence of $Zn^{\delta+}$ at the defective (stepped) Cu surface, which in the high-performance catalyst is a result of a dynamic SMSI effect leading to partial coverage of the metal particles with ZnO_x. Substitution of Zn into the Cu steps further strengthens the binding of the intermediates and increases the activity of the catalyst. The data presented suggest that the presence of steps and their close proximity to ZnO_x on the surface of the Cu particles create the ensemble needed to render the very active methanol copper: a Cu step with a nearby Zn serving as adsorption site for oxygen-bound intermediates.

These two requirements are fulfilled only for a small and varying fraction of the metallic Cu surface area, explaining the differences in intrinsic activity observed here and also in literature. Thus, under industrially relevant conditions a small fraction of the surface is largely contributing to the activity, which cannot be easily mimicked by simplified model approaches. We propose that the TOF of this reaction channel should be considerably higher compared with the values calculated on the basis of the full exposed Cu surface area.

References and Notes

1. G. A. Olah, A. Goeppert, G. K. Surya Prakash, *Beyond Oil and Gas: The Methanol Economy* (Wiley-VCH, Weinheim, Germany, 2006).
2. J. B. Hansen, P. E. Højlund Nielsen, in *Handbook of Heterogenous Catalysis*, G. Ertl, H. Knözinger, F. Schüth, J. Weitkamp, Eds. (Wiley-VCH, Weinheim, Germany, ed. 2, 2008), pp. 2920–2949.
3. M. S. Spencer, *Top. Catal.* **8**, 259 (1999).
4. I. Kasatkin, P. Kurr, B. Kniep, A. Trunschke, R. Schlögl, *Angew. Chem.* **119**, 7465 (2007).
5. M. Behrens, *J. Catal.* **267**, 24 (2009).
6. M. Kurtz, H. Wilmer, T. Genger, O. Hinrichsen, M. Muhler, *Catal. Lett.* **86**, 77 (2003).
7. The exposed Cu surface area can be measured using reactive chemisorption of N_2O, which leads to a surface oxidation of Cu ideally yielding a Cu_2O monolayer.
8. M. Kurtz *et al.*, *Catal. Lett.* **92**, 49 (2004).
9. J. Yoshihara, C. T. Campbell, *J. Catal.* **161**, 776 (1996).
10. P. B. Rasmussen *et al.*, *Catal. Lett.* **26**, 373 (1994).
11. J. Szanyi, D. W. Goodman, *Catal. Lett.* **10**, 383 (1991).
12. R. Burch, S. E. Golunski, M. S. Spencer, *J. Chem. Soc. Faraday Trans.* **86**, 2683 (1990).
13. Y. Kanai, T. Watanabe, T. Fujitani, T. Uchijima, J. Nakamura, *Catal. Today* **28**, 223 (1996).
14. K. Klier, *Adv. Catal.* **31**, 243 (1982).
15. V. Ponec, *Surf. Sci.* **272**, 111 (1992).
16. W. P. A. Jansen *et al.*, *J. Catal.* **210**, 229 (2002).
17. J. C. Frost, *Nature* **334**, 577 (1988).
18. J. Nakamura, Y. Choi, T. Fujitani, *Top. Catal.* **22**, 277 (2003).
19. K. C. Waugh, *Catal. Today* **15**, 51 (1992).
20. P. L. Hansen *et al.*, *Science* **295**, 2053 (2002).
21. M. M. Günter *et al.*, *Catal. Lett.* **71**, 37 (2001).
22. See supplementary materials on *Science* Online.
23. This effect arises from the generation of thin hexagonal domains in the cubic lattice with the change in stacking sequence of the hexagonally close-packed (111) layers at the stacking fault (ideal is A-B-C-A; stacking fault, A-B-C-B-C-A; twin boundaries, A-B-C-B-A). For more details and quantitative treatment see, e.g., (*24*).
24. B. E. Warren, *X-ray Diffraction* (Dover, New York, 1990).
25. G. C. Chinchen, P. J. Denny, J. R. Jennings, M. S. Spencer, K. C. Waugh, *Appl. Catal.* **36**, 1 (1988).
26. L. C. Grabow, M. Mavrikakis, *ACS Catal.* **1**, 365 (2011).
27. Z.-M. Hu, K. Takahashi, H. Nakatsuji, *Surf. Sci.* **442**, 90 (1999).
28. Y. Yang, J. Evans, J. A. Rodriguez, M. G. White, P. Liu, *Phys. Chem. Chem. Phys.* **12**, 9909 (2010).
29. Y. Morikawa, K. Iwata, K. Terakura, *Appl. Surf. Sci.* **169–170**, 11 (2001).
30. N.-Y. Topsøe, H. Topsøe, *Top. Catal.* **8**, 267 (1999).
31. R. Naumann d'Alnoncourt *et al.*, *Phys. Chem. Chem. Phys.* **8**, 1525 (2006).
32. J. D. Grunwaldt, A. M. Molenbroek, N. Y. Topsoe, H. Topsoe, B. S. Clausen, *J. Catal.* **194**, 452 (2000).
33. J. Słoczynski *et al.*, *Appl. Catal. A Gen.* **310**, 127 (2006).
34. I. A. Fisher, H. C. Woo, A. T. Bell, *Catal. Lett.* **44**, 11 (1997).

Acknowledgments: We thank M. Muhler and O. Hinrichsen for fruitful discussions. M.B., I.K., S.K., S.Z. F.G., and R.S. acknowledge the Bundesministerium für Bildung und Forschung (FKZ 01RI0529) and Süd-Chemie AG for financial support. P.K., B.-L.K., and R.W.F. thank the Bayerisches Wissenschaftsministerium (NW-0810-0002) for financial support of this work. F.S., F.A.-P., and J.K.N. wish to acknowledge support from the (U.S.) Department of Energy, Office of Basic Energy Sciences. The data presented in this work can be obtained from the corresponding authors upon request.

Supplementary Materials

www.sciencemag.org/cgi/content/full/science.1219831/DC1
Materials and Methods
Supplementary Text
Figs. S1 to S6
Tables S1 to S8
References (*35–52*)

30 January 2012; accepted 3 April 2012
Published online 19 April 2012;
10.1126/science.1219831

Structures of Cage, Prism, and Book Isomers of Water Hexamer from Broadband Rotational Spectroscopy

Cristóbal Pérez,[1] Matt T. Muckle,[1] Daniel P. Zaleski,[1] Nathan A. Seifert,[1] Berhane Temelso,[2] George C. Shields,[2]* Zbigniew Kisiel,[3]* Brooks H. Pate[1]*

Theory predicts the water hexamer to be the smallest water cluster with a three-dimensional hydrogen-bonding network as its minimum energy structure. There are several possible low-energy isomers, and calculations with different methods and basis sets assign them different relative stabilities. Previous experimental work has provided evidence for the cage, book, and cyclic isomers, but no experiment has identified multiple coexisting structures. Here, we report that broadband rotational spectroscopy in a pulsed supersonic expansion unambiguously identifies all three isomers; we determined their oxygen framework structures by means of oxygen-18–substituted water ($H_2{}^{18}O$). Relative isomer populations at different expansion conditions establish that the cage isomer is the minimum energy structure. Rotational spectra consistent with predicted heptamer and nonamer structures have also been identified.

The intermolecular hydrogen-bonding interactions of water are responsible for many remarkable physical properties of the liquid and solid phases of the compound and furthermore play a pivotal role in solution chemistry and biochemistry. As a result, the accurate description of the water intermolecular potential is one of the most important problems in chemistry (*1*). One key method for quantitative analysis of water interactions is the size-selective study of the structures of water clusters (*2–5*). This problem has been attacked using several state-of-the-art techniques, including far-infrared (FIR) spectroscopy (*6–9*), helium nanodroplet isolation (HENDI) spectroscopy (*10*), infrared spectroscopy of size-selected molecular beams (*11*), molecular tagging ion-dip infrared spectroscopy (*12*, *13*), and argon-mediated, population-modulated attachment spectroscopy (*14*). Here, we report chirped-pulse Fourier transform microwave

(CP-FTMW) spectra (*15*) of clusters produced in a pulsed supersonic expansion. We thereby identify three isomers of the water hexamer, obtain direct structural information on these isomers through the analysis of isotopically labeled clusters, and establish that the cage structure is the global minimum.

The water hexamer has become a benchmark problem for computational chemistry (*16*–*22*). Theoretical studies of water cluster structures indicate that the hexamer is a special cluster size wherein three-dimensional structures become more stable than the planar ring structures found for the smaller clusters (*2*, *3*), a result supported by experimental studies of size-specific clusters of water on benzene (*12*). For this transitional cluster, there is a complex, multidimensional potential energy surface, and several low-energy structural isomers are predicted, including prism, cage, book, bag, and cyclic forms. There is consensus among the most recent calculations that the prism, cage, and book isomers are the three lowest energy isomers, with an energy separation of 1 kJ/mol or less when zero-point corrections are included (*16*, *20*). The prism has been calculated to be the lowest-energy isomer, although the prism and cage are nearly isoenergetic, and the book is slightly higher in energy.

Experimental studies of the water hexamer have identified the cage, book, and cyclic isomers based on the comparison of calculated and observed spectral properties. The hitherto most definitive structure identification has been the observation of the cage by high-resolution FIR spectroscopy (*9*). The experimental rotational constants, which measure the mass distribution in the cluster through the principal moments of inertia, were consistent only with theoretical calculations of the cage structure. The tunneling splitting patterns and dipole moment of the cluster were subsequently shown to be consistent with the theoretical predictions for the cage structure as well (*23*). No other isomers were detected. A higher-energy cyclic isomer of the water hexamer, produced under the unique cluster growth conditions of helium nanodroplets, was identified by HENDI spectroscopy (*10*) from the frequency of a vibrational band of the O-H stretch that followed the theoretical prediction for red shift as a function of cluster size. In two experiments in which the infrared spectrum in the region of the O-H stretch was measured for water hexamer clusters produced in a supersonic expansion (*11*, *14*), the comparison to theoretical spectra indicated the presence of the book isomer. In the case of the study using size-selected molecular beams (*11*), the dominance of the book isomer, which is entropically favored over the cage and prism isomers (*16*), was consistent with the warmer temperature of the sample (40 K) in these measurements compared with the slit-jet FIR spectroscopy measurements (6 K) and the HENDI experiments (0.38 K). However, recent theoretical calculations of hexamer vibrational spectra have suggested that the assignment of the book isomer may need to be revisited (*24*).

The structures of water clusters have presently been characterized by analysis of their rotational spectra. Molecular rotational spectroscopy, applicable to polar molecules in the gas phase, is one of the most exacting experimental techniques for characterizing molecular structure. Analysis of the rotational spectrum permits a high-accuracy determination of the principal moments of inertia. This accuracy is needed for structure determination using isotopic substitution because the small differences in the moments of inertia of the naturally abundant and isotopically labeled analogs are used to obtain the atom positions. The high spectral resolution of pulsed-jet microwave spectroscopy is crucial for structure determination by isotopic substitution, where it is necessary to fully resolve the several closely spaced rotational spectra of each isotopolog in the sample. The rotational spectra were measured in a CP-FTMW spectrometer with frequency coverage from 7 to 18 GHz (*15*). Separate broadband rotational spectra were recorded by flowing argon, neon, and helium over an external reservoir of water at room temperature. In addition, a measurement using neon as the carrier gas was performed using a water sample that contained 15% $H_2{}^{18}O$. The CP-FTMW data and detailed analysis of all spectra are provided in the supplementary materials.

The broadband rotational spectrum of water is shown in Fig. 1. The rotational spectrum of the water dimer (*25*) is the most intense contributor. The minimum energy structures of the water trimer, tetramer, and pentamer are effectively nonpolar in their ground states, so these clusters cannot be observed. The previously identified cage isomer of the water hexamer (*9*) gives the next strongest spectrum, observed at about a 200:1 signal-to-noise ratio in neon. Spectra for the prism and book isomers are about half as intense. The prism isomer is the only one to show fine structure associated with the rearrangement of the hydrogen-bond network through tunneling. We have also assigned rotational spectra that we attribute to a water heptamer and a water nonamer cluster, based on comparison to the rotational constants from theoretical structures (*16*). The structures are tentatively identified as the heptamer PR1 and nonamer D2dDD in the nomenclature of (*16*). The two most stable cubic structures of the octamer are nonpolar (*13*). A summary of the spectroscopic constants of these water clusters and comparison to the rotational constants predicted by electronic structure theory are given in Table 1. For the prism, the rotational constants reported in Table 1 are obtained from a fit of the center frequencies of the observed tunneling fine structure.

The rotational spectrum was measured using different inert carrier gases to gain information about the relative stability of the water hexamer isomers based on their population in the molecular expansion, as shown in Fig. 2. The electric dipole moment of the cluster is required to convert the spectral intensities to populations and

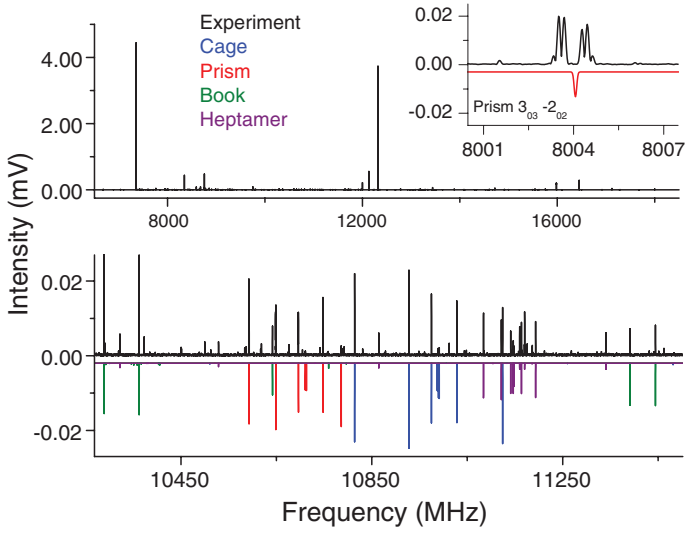

Fig. 1. The black traces show different views of the experimental CP-FTMW pulsed-jet spectrum of water using neon backing gas. The final spectrum is obtained from the signal average of 650,000 free induction decay (FID) measurements with a 20-μs gate duration. The colored traces in the bottom panel are 1.5 K (rotational temperature) simulations of the hexamer cage (blue), hexamer prism (red), hexamer book (green), and heptamer (purple). The nonamer is not seen on this scale but can be found in fig. S6. The inset in the top panel shows the 3_{03}-2_{02} rotational transition (defined using the standard nomenclature for the quantized rotational energy levels of an asymmetric top denoted J_{KaKc}, where J is the quantum number for the total rotational angular momentum and K_a and K_c are the quantum numbers for the projection of total rotational angular momentum onto the a- and c-principal rotation axes, respectively) of the prism isomer, highlighting the structure due to quantum tunneling. The simulation of the prism, shown in red, has been fit to the line centers.

[1]Department of Chemistry, University of Virginia, McCormick Road, Charlottesville, VA 22903, USA. [2]Dean's Office, College of Arts and Sciences and Department of Chemistry, Bucknell University, Lewisburg, PA 17837, USA. [3]Institute of Physics, Polish Academy of Sciences, Aleja Lotników 32/46, 02-668 Warszawa, Poland.

*To whom correspondence should be addressed. E-mail: brookspate@virginia.edu (B.H.P.); george.shields@bucknell.edu (G.C.S.); kisiel@ifpan.edu.pl (Z.K.)

the analysis uses ab initio estimates of the dipole moments reported in table S41. The estimated population ratio for cage:prism:book is 1:1:0.25 in neon and helium. However, in an argon expansion, only the cage isomer is observed (with a signal-to-noise ratio of 50:1), giving strong evidence that the cage is the global minimum energy structure for the water hexamer, as inferred in the previous FIR spectroscopy work (*9*). The mechanism for the enhanced cooling efficiency of heavier carrier gases in free-jet expansions has been recently discussed (*26*). The prism, often found to be the lowest-energy isomer in calculations using high-level quantum chemistry (*3*, *16*, *18*–*22*), is the next-lowest-energy isomer based on this population analysis. The spectra attributed to heptamer and nonamer water clusters are observed in all three carrier gases, indicating that these are the global minimum configurations.

Although the agreement between experimental and theoretical spectroscopic constants provides compelling support for the identification of the cage, prism, and book isomers, the study of isotopically labeled water clusters gives unambiguous structure identification. As shown in Fig. 2, using an $H_2{}^{18}O$-enriched sample leads to the assignment of six separate rotational spectra, each with a single $H_2{}^{18}O$ molecule incorporated into a structurally unique site of the cluster. For the prism, only six distinct spectra were identified, and none of them show the fine structure observed in the normal $H_2{}^{16}O$ cluster spectrum. This result supports the attribution of this fine structure to tunneling between several identical minima of the potential energy surface. Upon substitution by a single $H_2{}^{18}O$ molecule in the cluster, these minima are no longer energetically equivalent and the quantum tunneling is quenched. One implication of this result is that the tunneling dynamics observed for the prism are not the bifurcation pathways that are the focus of previous analysis of FIR spectra because these motions would still connect equivalent minima of the potential energy surface upon single ^{18}O substitution (*23*).

The initial structural analysis of the water hexamers uses the method of Kraitchman, in which the oxygen atom framework is built up atom by atom by converting the changes in the moments of inertia upon isotopic substitution into atom coordinates in the principal axis system to construct the so-called substitution structure (*27*). The relative signs of the atom coordinates are the only additional parameters needed in this analysis, and they are assigned based on the ab initio cluster geometries (*16*). The substitution structures of the water hexamer isomers are compared to theoretical structures, which include vibrational averaging, in the top panel of Fig. 3. Zero-point vibrationally averaged structures are calculated using vibrational perturbation theory (VPT2) applied on the second-order Møller-Plesset perturbation theory (MP2) potential energy surface (*28*, *29*). In VPT2, the cubic and semidiagonal quartic force constants are computed by finite differentiation of the Hessian along the normal mode coordinates and are used to obtain the vibrationally averaged structure of a cluster at 0 K. A comparison of the vibrationally averaged and equilibrium theoretical geometries is shown in figs. S11 to S15. The direct Kraitchman analysis is sufficient to unambiguously identify the prism, cage, and book isomers.

However, the Kraitchman method is unreliable for quantitative analysis when atoms are close to the principal axes because of zero-point vibrational contributions to the moments of inertia that vary upon isotopic substitution. As detailed in the supplementary materials (tables S32, S35, and S38), each water hexamer isomer has two individual principal axis components that return unphysical values (out of the 18 total Cartesian coordinates that define the oxygen atom framework for a hexamer). An alternative means of analysis is to fit the structure directly to the complete set of isotopic rotational constants to determine the effective ground-state geometry, the so-called r_0 structure (*30*). The oxygen framework of 6 atoms is defined by $3N-6=12$ internal coordinates, and 21 experimental moments of inertia are available, so there is a sufficient number of degrees of freedom to fit the complete oxygen framework. Because the present experimental results carry only a limited amount of information on the positions of the hydrogen atoms, additional assumptions are required. The specific assumptions are not critical, but the lowest deviations of fits were obtained in the r_0 analysis assuming the experimental r_0 monomer geometry for each water unit (*31*). In addition, the orientations of the water molecules in the cluster are based on the vibrationally averaged theoretical structures in a way that keeps the angles of the strongest hydrogen bonds constant. The experimental r_0-structure oxygen atom frameworks are compared with the vibrationally averaged theoretical structures in the bottom panel of Fig. 3.

A detailed comparison of the experimental and theoretical O···O bond distances is given in Fig. 4. There is remarkable agreement between experiment and computations concerning the variation in O···O bond distances within each cluster isomer, allowing more confident, detailed insight into the hydrogen-bonding network for each isomer. The O···O distance is a known measure of hydrogen bond strength, and in the hexamer isomers these span the range 2.70 to 3.01 Å. This is a departure from the more uniform picture for the global minimum clusters up to the water pentamer in which symmetry enforces a single O···O distance, systematically decreasing with cluster size (*4*). The shortest O···O distance in the hexamers is shorter than the 2.76 Å separation of the pentamer, whereas the longest hexamer O···O distance exceeds the value found for the water dimer, 2.98 Å (*4*). The detachment energy of

Table 1. Experimental and calculated rotational constants for observed $(H_2{}^{16}O)_n$ clusters.

	Experimental	Theory	
		Equilibrium*	Vibrationally averaged
Hexamer cage			
A/MHz	2161.8762(8)	2249.2†	2172.4†
B/MHz	1129.3153(5)	1149.8	1129.2
C/MHz	1066.9627(5)	1097.9	1070.3
Hexamer prism			
A/MHz	1658.224(4)	1697.2	1644.5
B/MHz	1362.000(2)	1416.6	1373.6
C/MHz	1313.124(2)	1358.3	1312.5
Hexamer book			
A/MHz	1879.4748(8)	1898.3	1856.1
B/MHz	1063.9814(6)	1106.3	1080.5
C/MHz	775.0619(3)	809.5	788.7
Heptamer PR1			
A/MHz	1304.4355(3)	1333.7	1297.5
B/MHz	937.8844(6)	974.1	950.7
C/MHz	919.5236(6)	954.2	926.8
Nonamer D2dDD			
A/MHz	774.7442(7)	810.9	791.2
B/MHz	633.5403(6)	630.6	619.8
C/MHz	570.6460(5)	585.9	574.1

*From (*16*). †Distinct cage configurations are labeled according to the up(u) or down(d) position of the two free hydrogens of the edge (single donor-single acceptor) waters about the most immediate O-O-O plane. The calculated rotational constants are for the uu{1} structure, which is practically isoenergetic with the du{1} structure considered in (*16*) and is currently preferred on the basis of comparison between relative values of experimental and calculated dipole moment components and the deviations of the structural fits. See section 3.1 in the supplementary materials.

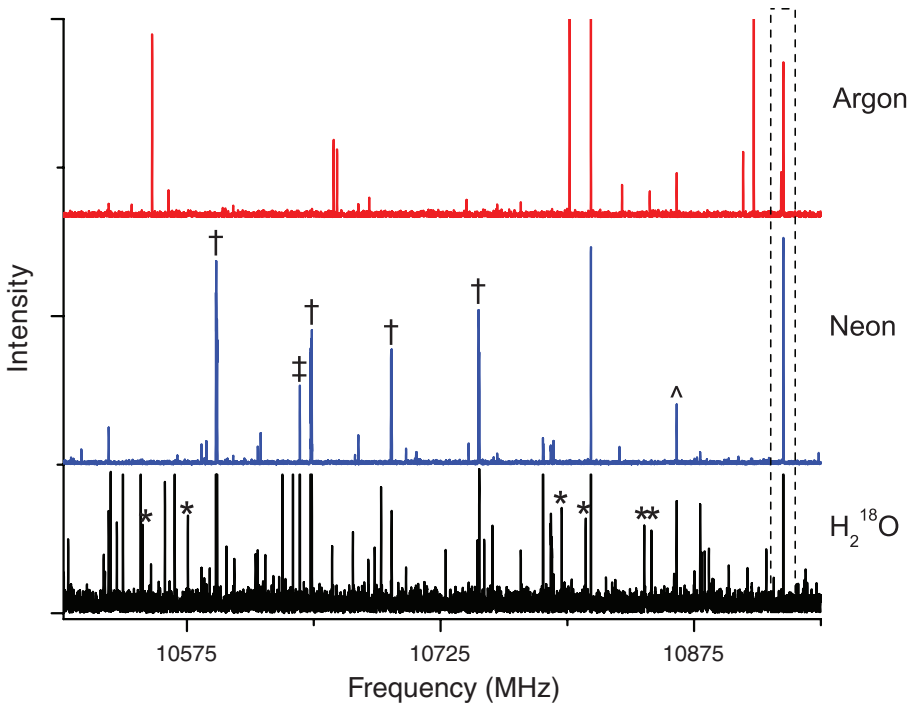

Fig. 2. The black trace shows a portion of the $H_2{}^{18}O$-enriched (15%) CP-FTMW spectrum obtained by averaging 550,000 FID signals. The offset blue trace shows the same region in the $H_2{}^{16}O$ cluster spectrum (average of 650,000 FID signals) measured with a neon backing gas. The offset red trace shows the same region (average of 200,000 FID signals) measured with an argon backing gas. The dashed box shows the 5_{05}-4_{04} rotational transition of the hexamer-cage isomer (intensity going off scale). The asterisks show the six individual $K_a = 0$ transitions resulting from isotopic substitution. The transitions marked with daggers indicate transitions assigned to the hexamer prism. The transition marked by the double dagger indicates a transition assigned to the hexamer book. The hexamer cage is the only isomer observed when argon is used as a backing gas, indicating that the cage is the lowest-energy isomer of the water hexamer. Similar data for the hexamer prism (fig. S4) and hexamer book (fig. S5) can be found in the supplementary materials. Finally, the caret indicates a transition belonging to the heptamer, whose presence remains when the backing gas is argon.

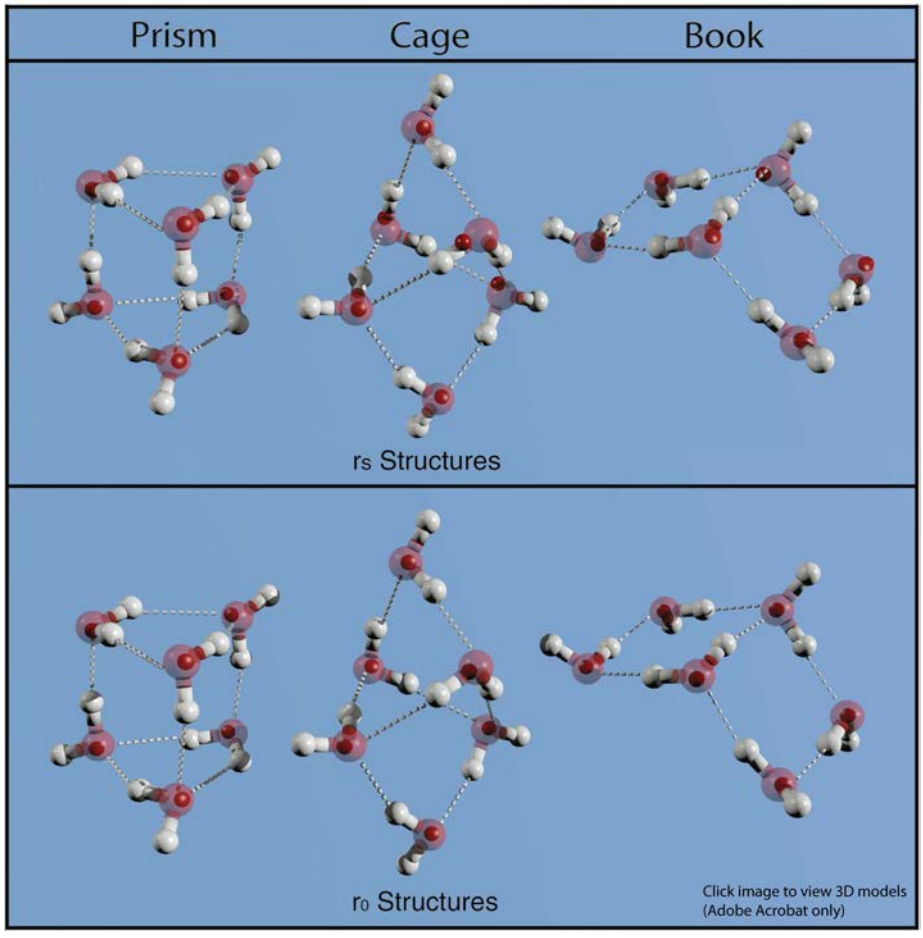

Fig. 3. The experimental structures of the water hexamer isomers determined using Kraitchman analysis (top, the substitution structure, r_s) and r_0 analysis (bottom) are compared with the vibrationally averaged ab initio structures. The full molecular structure rendering is the theoretical structure with lines drawn to denote the hydrogen-bonding network. The smaller dark red spheres are the experimental atom positions for the oxygen framework. Note the improved agreement in the oxygen atom positions for the r_0 analysis.

each water molecule in the cluster is also given in Fig. 4. This quantity was calculated with the density-fitted second-order Møller–Plesset perturbation theory with F12 explicit correlation factor employing a correlation consistent valence triple-zeta basis set (DF-MP2-F12/VTZ-F12) method (*32*), as detailed in the supplementary materials (section 1.2). The water detachment energies show large variation but correlate with the O···O distances and with the number of hydrogen bonds to each water monomer. This provides a consistent picture of the diversity of

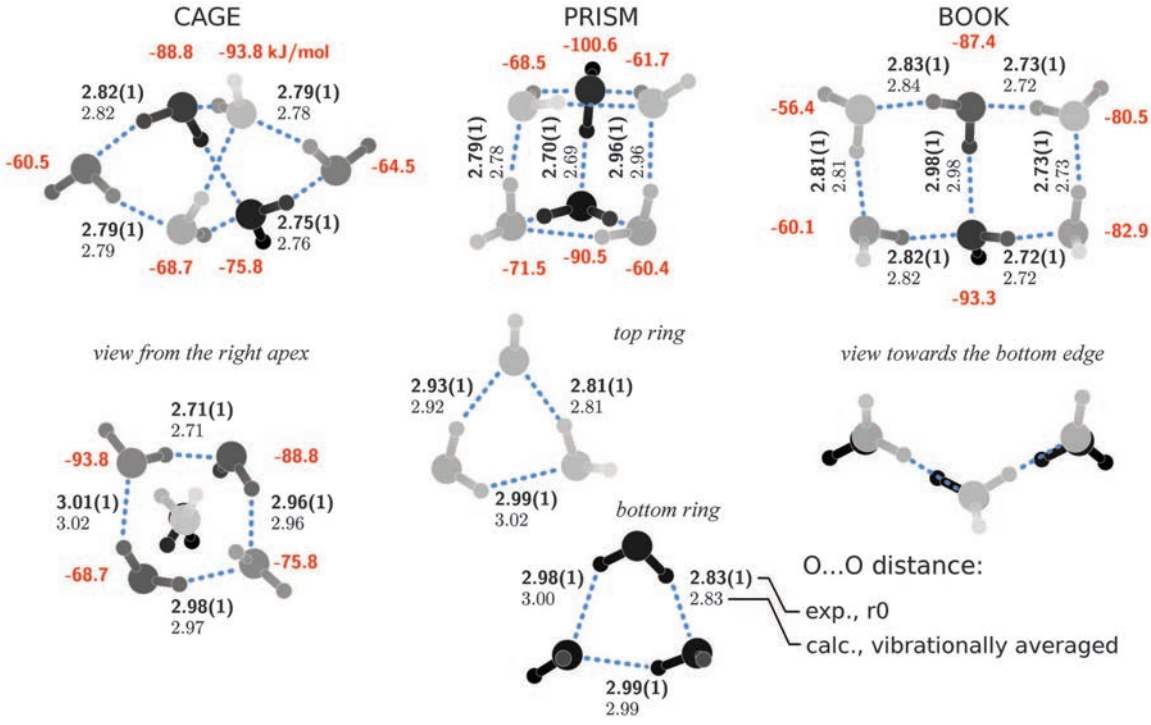

Fig. 4. The experimental r_0-analysis structures are shown for the three water hexamer isomers. The dashed lines indicate the hydrogen-bonding network. The experimental O···O bond distances, in Angstroms, are given in bold with the theoretical values from the vibrationally averaged structures below. The detachment energy for each water molecule in the cluster is given in red.

hydrogen bonding appearing at the hexamer cluster level and is a small-scale prelude to the known diversity in the structure of liquid water.

References and Notes

1. R. Bukowski, K. Szalewicz, G. C. Groenenboom, A. van der Avoird, *Science* **315**, 1249 (2007).
2. J. K. Gregory, D. C. Clary, *J. Phys. Chem.* **100**, 18014 (1996).
3. S. S. Xantheas, C. J. Burnham, R. J. Harrison, *J. Chem. Phys.* **116**, 1493 (2002).
4. K. Liu, J. D. Cruzan, R. J. Saykally, *Science* **271**, 929 (1996).
5. F. N. Keutsch, R. J. Saykally, *Proc. Natl. Acad. Sci. U.S.A.* **98**, 10533 (2001).
6. N. Pugliano, R. J. Saykally, *Science* **257**, 1937 (1992).
7. J. D. Cruzan *et al.*, *Science* **271**, 59 (1996).
8. K. Liu, M. G. Brown, J. D. Cruzan, R. J. Saykally, *Science* **271**, 62 (1996).
9. K. Liu *et al.*, *Nature* **381**, 501 (1996).
10. K. Nauta, R. E. Miller, *Science* **287**, 293 (2000).
11. C. Steinbach *et al.*, *Phys. Chem. Chem. Phys.* **6**, 3320 (2004).
12. R. N. Pribble, T. S. Zwier, *Science* **265**, 75 (1994).
13. C. J. Gruenloh *et al.*, *Science* **276**, 1678 (1997).
14. E. G. Diken, W. H. Robertson, M. A. Johnson, *J. Phys. Chem. A* **108**, 64 (2004).
15. G. G. Brown *et al.*, *Rev. Sci. Instrum.* **79**, 053103 (2008).
16. B. Temelso, K. A. Archer, G. C. Shields, *J. Phys. Chem. A* **115**, 12034 (2011).
17. U. Góra, R. Podeszwa, W. Cencek, K. Szalewicz, *J. Chem. Phys.* **135**, 224102 (2011).
18. G. Hincapié, N. Acelas, M. Castaño, J. David, A. Restrepo, *J. Phys. Chem. A* **114**, 7809 (2010).
19. Y. Chen, H. Li, *J. Phys. Chem. A* **114**, 11719 (2010).
20. D. M. Bates, G. S. Tschumper, *J. Phys. Chem. A* **113**, 3555 (2009).
21. E. E. Dahlke, R. M. Olson, H. R. Leverentz, D. G. Truhlar, *J. Phys. Chem. A* **112**, 3976 (2008).
22. B. Santra *et al.*, *J. Chem. Phys.* **129**, 194111 (2008).
23. K. Liu, M. G. Brown, R. J. Saykally, *J. Phys. Chem. A* **101**, 8995 (1997).
24. Y. Wang, J. M. Bowman, *J. Chem. Phys.* **134**, 154510 (2011).
25. E. Zwart, J. J. ter Meulen, W. Leo Meerts, L. H. Coudert, *J. Mol. Spec.* **147**, 27 (1991).
26. U. Erlekam, M. Frankowski, G. von Helden, G. Meijer, *Phys. Chem. Chem. Phys.* **9**, 3786 (2007).
27. J. Kraitchman, *Am. J. Phys.* **21**, 17 (1953).
28. V. Barone, *J. Chem. Phys.* **122**, 014108 (2005).
29. M. J. Frisch *et al.*, Gaussian 09 (Gaussian, Inc., Wellington, CT, 2009).
30. Z. Kisiel, *J. Mol. Spec.* **218**, 58 (2003).
31. F. C. De Lucia, P. Helminger, W. Gordy, H. Morgan, P. Staats, *Phys. Rev. A* **8**, 2785 (1973).
32. H. J. Werner, T. B. Adler, F. R. Manby, *J. Chem. Phys.* **126**, 164102 (2007).

Acknowledgments: This work was supported by U.S. National Science Foundation (NSF) grants CHE-0960074 and CHE-0848827; the Institute of Physics, Polish Academy of Sciences; and NSF grants CHE-0116435, CHE-0521063, and CHE-0849677 as part of the MERCURY high-performance computer consortium (www.mercuryconsortium.org). This research used the NSF TeraGrid resources provided by the Texas Advanced Computing Center (TACC) under grant TG-CHE090095 and resources of the National Energy Research Scientific Computing Center, which is supported by the Office of Science of the U.S. Department of Energy under contract DE-AC02-05CH11231.

Supplementary Materials

www.sciencemag.org/cgi/content/full/336/6083/897/DC1
Materials and Methods
Figs. S1 to S15
Tables S1 to S46
References (*33*–*62*)

15 February 2012; accepted 23 March 2012
10.1126/science.1220574

Observation of ^{239}Pu Nuclear Magnetic Resonance

H. Yasuoka,[1,2] G. Koutroulakis,[1]* H. Chudo,[1,2] S. Richmond,[1] D. K. Veirs,[1] A. I. Smith,[1] E. D. Bauer,[1] J. D. Thompson,[1] G. D. Jarvinen,[1] D. L. Clark[1]

In principle, the spin-½ plutonium-239 (^{239}Pu) nucleus should be active in nuclear magnetic resonance spectroscopy. However, its signal has eluded detection for the past 50 years. Here, we report observation of a ^{239}Pu resonance from a solid sample of plutonium dioxide (PuO_2) subjected to a wide scan of external magnetic field values (3 to 8 tesla) at a temperature of 4 kelvin. By mapping the external field dependence of the measured resonance frequency, we determined the nuclear gyromagnetic ratio $^{239}\gamma_n(PuO_2)/2\pi$ to be 2.856 ± 0.001 megahertz per tesla (MHz/T). Assuming a free-ion value for the Pu^{4+} hyperfine coupling constant, we estimated a bare $^{239}\gamma_n/2\pi$ value of ~2.29 MHz/T, corresponding to a nuclear magnetic moment of $\mu_n \approx 0.15\mu_N$ (where μ_N is the nuclear magneton).

Since its discovery by Bloch and Purcell in 1946 (*1*, *2*), nuclear magnetic resonance (NMR) spectroscopy has evolved into an indispensable tool for experimental condensed matter physics, the determination of molecular structure, the study of molecular dynamics, and the characterization of atoms and molecules in the gaseous, liquid, and solid state. NMR is predicated on the fact that a nucleus with a nonzero spin angular momentum **I** possesses a magnetic